Determination of the seismic structure of the Earth based on joint analysis of gravimetric and seismometric data – a case study

Kamila Karkowska[1], Monika Wilde-Piórko[2], Przemysław Dykowski[3], Marcin Sękowski[4], Marcin Polkowski[5]

[1] *Polish Geological Institute – National Research Institute, Warsaw, Poland,*
e-mail: kamila.karkowska@pgi.gov.pl (corresponding author), ORCID ID: 0000-0001-7039-7718
[2] *Institute of Geodesy and Cartography, Warsaw, Poland, ORCID ID: 0000-0001-7347-4766*
[3] *Institute of Geodesy and Cartography, Warsaw, Poland; Central Office of Measures, Warsaw, Poland,*
ORCID ID: 0000-0002-9092-9926
[4] *Institute of Geodesy and Cartography, Warsaw, Poland, ORCID ID: 0000-0002-9702-5890*
[5] *Accenture, Applied Intelligence, USA*

Abstract: The evolution of the Earth's surface is driven by external and internal forces, the latter of which can only be studied indirectly. Knowledge about the structure of the Earth's interior is very important for modeling and predicting the processes occurring at the surface. This study presents a new concept of joint analysis of the gravimetric and seismometric recordings of earthquakes for determining the seismic structure of the Earth down to the depth of 1250 km. The proposed method allows the use of gravimetric data without the known full transfer function of the instrument. Group velocity dispersion curves of the fundamental mode of Rayleigh waves up to the period of 550 s are measured based on the joint analysis of the recordings of superconducting gravimeter and broadband seismometers operating at the same location in five testing sites in Europe, allowing for the exploration of a broader response for incoming seismic waves. Averaged dispersion curves for earthquakes around the world for each site are inverted by the weighted linear inversion and Monte Carlo methods to estimate the distribution of shear-wave seismic velocity in the Earth's mantle. A comparison of the deterministic and probabilistic inversion methods can excellently demonstrate surface waves' ability to determine the Earth's mantle structure. The inversion results are compared with the global ak135 seismic model (Kennett et al. 1995) to verify the proposed method.

Keywords: superconducting gravimeters, broad-band seismometers, Rayleigh waves, linear inversion, Monte Caro inversion

INTRODUCTION

Knowledge of the structure of the Earth's interior and processes occurring in it are very important when studying the phenomena forming the Earth's surface. Studies of the seismic structure of the Earth's crust and upper mantle based on the analysis of surface waveforms generated by earthquakes were developed intensively in the 1950s and 1960s. A theory of surface wave propagation, computation techniques, measuring of surface wave parameters and method for their quantitative interpretation was presented e.g., by Keilis-Borok (1989). The progress in the determination of the

global and regional structure of the Earth based on analysis of teleseismic and regional surface wave data was described by Romanowicz (2002).

The group and/or phase velocities of surface waves can be measured and used to deduce the elastic properties of the crust and mantle structure. Various inversion strategies are being adopted to determine the Earth's seismic structure based on surface wave dispersion curves. Generally, they can be classified as deterministic (LIN) or probabilistic (MC) methods. The first group of methods are based on an iterative linearized least square procedure (e.g., Lyu et al. 2017), and the second group uses the Monte Carlo approach (e.g., Shapiro et al. 2000, Gaudot et al. 2021). In the LIN methods, the best Earth's structure model is obtained using an iterative procedure starting from an initial model, progressively adjusted by minimizing the misfit function, which measures the discrepancy between the data and prediction (e.g., Herrmann & Ammon 2004). Generally, in such local search methods, the initial model may significantly impact the result, so the optimal choice of this model is crucial. What is more, due to the assumption of linear inversion, the initial model should be close to the true structure. In MC methods, the result is not represented by a single model but by a large set of models sampling the posterior probability density function (e.g., Bodin et al. 2012). The MC methods can search a wide range of model parameters to find those for which the probability density function attains significant values. There have also been combinations of the above two methods proposed. The result of the LIN method is taken to reduce the searched parameter space in the MC method (e.g., Martínez et al. 2005, Peter et al. 2008) or vice versa, where the most probable model obtained from MC inversion is used as a starting model for LIN inversion (e.g., Köhler et al. 2015). Also, the merging of features of the above methods have been implemented, e.g. by Kolínský et al. (2014) in an isometric method.

However, no matter what inversion strategy is used, the depth range of the resulting model mainly depends on the period range of the analysed dispersion curves of surface waves. Typically, the maximum period of surface waves recorded by broad-band seismometers analysed is 100 s, allowing the estimate of seismic structure down to a depth of 200–250 km (e.g., Köhler et al. 2015, Lyu et al. 2017). To obtain information about deeper mantle structure, the recording of waves of longer periods has to be analysed, or a joint inversion of the fundamental and higher modes of surface waves can be applied (e.g., Debayle & Ricard 2012). Higher modes are more sensitive to deeper structures but, on the other hand, more challenging to measure. An example of an analysis of long period seismic waves was presented by Peter et al. (2008). The shear-wave (S-wave) velocity model down to the depth of 400 km for the European-Mediterranean region was determined based on the seismometric data for a period range of 35–300 s. However, Bormann et al. (2012) pointed out that it is possible to estimate the S-wave velocity structure of the Earth, even down to the lower mantle, when surface wave dispersion curves up to the periods of 500 s are inverted.

Modern tidal gravimeters can record relative global and local acceleration changes due to gravity. They are characterized by a flat transfer function and constant scale factor for frequencies lower than 5–10 mHz (100–200 s). Typical broad-band seismometers record the Earth's surface velocities without amplitude distortions in the frequency range from 8.3 mHz to 50 Hz (0.02–120 s). The range of frequencies of ground motion caused by earthquake waves extends from 0.3 mHz (~3300 s), so there are recording frequencies which are largely distorted by seismometers, and very little distorted by gravimeters, giving a unique opportunity for studying very long-period surface waves. It should be emphasized that both types of sensors can provide the same information for any ground motion above their noise level and below their saturation level because they are equipped with inertial sensors which are sensitive to acceleration.

A detailed analysis of earthquake recordings by gravimeter compared to broad-band seismometric ones has been presented by Karkowska et al. (2022a). Also, the transfer function of these systems has been analysed in detail, and a simple processing scheme of gravimetric data has been proposed in a period range of 10–1000 s. Furthermore, the Earth's seismic structure based on intermediate-period surface wave recordings of tidal gravimeters was estimated by Karkowska

et al. (2022b) on a regional scale by weighted linear inversion methods. Additionally, a comprehensive approach to the quantitative evaluation of inverted models was presented to show the capabilities of the gravimetric data to retrieve the S-wave velocity distribution with depth.

This paper presents a novel concept of joint analysis of gravimetric and seismometric data to improve the determination of the Earth's structure. Group-velocity dispersion curves of fundamental-mode Rayleigh waves are measured from recordings of tidal gravimeters and broad-band seismometers, operating at the same location, allowing for the exploration of a broader response for incoming seismic waves. One joint group-velocity dispersion curve of Rayleigh surface waves is estimated for each selected European site. A comparison of the deterministic and probabilistic inversion methods excellently demonstrates the ability of surface waves to determine the Earth's structure. Due to the applied procedure using the worldwide distribution of earthquakes, the obtained inversion models should be closed by the 1-D global model of the seismic Earth's structure. The inversion results are compared with the global ak135 seismic model (Kennett et al. 1995) to verify the proposed method.

DATA AND METHODOLOGY

Five European stations with a collocated broadband seismometer (BB) and superconducting gravimeter (SG) installed in the same observatories were chosen for the case study. The only exception is a site in Spain, where the distance between instruments is about 27 km. The gravimeter is located at the Yebes Observatory, while the closest seismometer is located at the ROA/UCM Station Universidad Complutense Madrid. For simplicity's sake, the site will hereafter be called Yebes. The choice of these stations allows for the verification of proposed method for using recordings of various types of seismometers and gravimeters (including also the testing of different data's sample rates). Selected stations with instrument types and coordinates are summarised in Table 1, and their location across Europe is presented in Figure 1.

The selected sites are located along a profile running from the western Mediterranean (Spain) to Central Europe (Poland), crossing a complex tectonic setting – an assemblage of Phanerozoic and Precambrian units, separated by the Teisseyre–Tornquist Zone (TTZ, see Fig. 1) (e.g., Dercourt et al. 1986, Pharaoh 1999).

Table 1
List of selected stations with coordinates, types of instruments, codes, period of analysed data and number of events

| Station	Coordinates		Gravimeters			Seismometers		
	latitude	longitude	instrument (IGETS code)	period of analysed data	no. of events	instrument (IRIS code)	period of analysed data	no. of events
Yebes (*ROA/UCM*)	40.5238 (*40.3075*)	−3.0902 (*−3.2441*)	GWR OSG064 (ys064)	05.2016–03.2020	1114	STS-2 (WM.UCM)	11.2016–03.2020	788
Larzac	43.9700	3.2220	GWR iGrav002 (la002)	11.2016–12.2018	619	STS-2 (FR.LAJAS)	07.2017–09.2019	413
Wettzell	49.1440	12.8780	GWR CD029 (we029-1)	07.2013–03.2018	1798	STS-2 (GR.WET)	07.2013–03.2020	2299
Pecny	49.9141	14.7868	GWR OSG050 (pe050)	07.2013–03.2020	2297	Guralp CMG3T (CZ.GOPC)	07.2013–11.2018	1050
Borowa Góra	52.4755	21.0359	GWR iGrav027 (bg027)	01.2017–12.2020	1317	REF-TEK 151B-120	12.2016–12.2020	1227
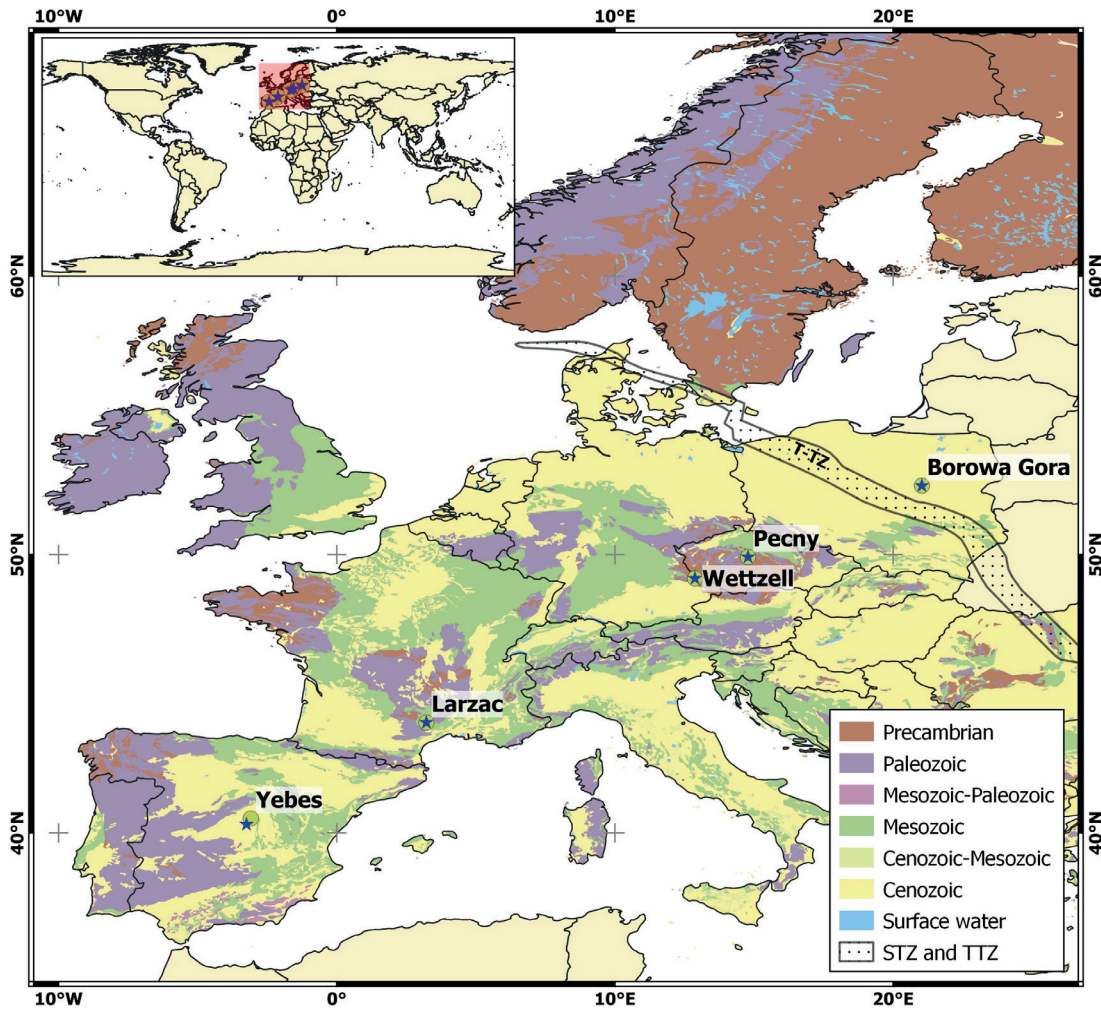
Fig. 1. *Location of selected stations on a generalised geological map of Europe (Pawlewicz et al. 2003) with the Teisseyre–Tornquist Zone (TTZ) by Pharaoh (1999); location of gravimetric stations are marked by stars and seismic ones by dots*

The TTZ divides Europe into a seismically slow region to the west and a seismically fast region to the east (e.g., Peter et al. 2008, Schivardi & Morelli 2011). These facts are closely related to the structure of the tectonic units. Crust and lithosphere thickness in Europe varies, as described e.g., by the CRUST1.0 model of Laske et al. (2013) and by the LITHO1.0 model by Pasyanos et al. (2014), respectively. The depth of the boundary between the crust and the mantle (Moho) increases from 26–30 km for the Yebes and Larzac stations, through 30–34 km for the Wettzell and Pecny stations, to 42 km for the Borowa Góra station (Fig. 2). The depth of the upper boundary of the asthenospheric mantle is relatively low for the Yebes, Larzac, Wettzell, and Pecny stations (called later Phanerozoic stations),

in the range of 50–90 km, compared to the Borowa Góra station (later called a Precambrian station), where it reaches a depth of 230 km (Fig. 2).

Schivardi & Morelli (2011) have presented the EPmantle model, a 3-D transversely isotropic shear wave velocity model of the European Plate down to the depth of 300 km, obtained by analysis of fundamental mode Rayleigh and Love group velocity measurements. Along the profile from this study, they generally observed negative relative shear velocity anomalies of magnitude in the range from −0.5% to −3% for the Phanerozoic stations and positive anomalies of magnitude in the range of 0.5–2% for the Precambrian station with respect to the global PREM model (Dziewonski & Anderson 1981).
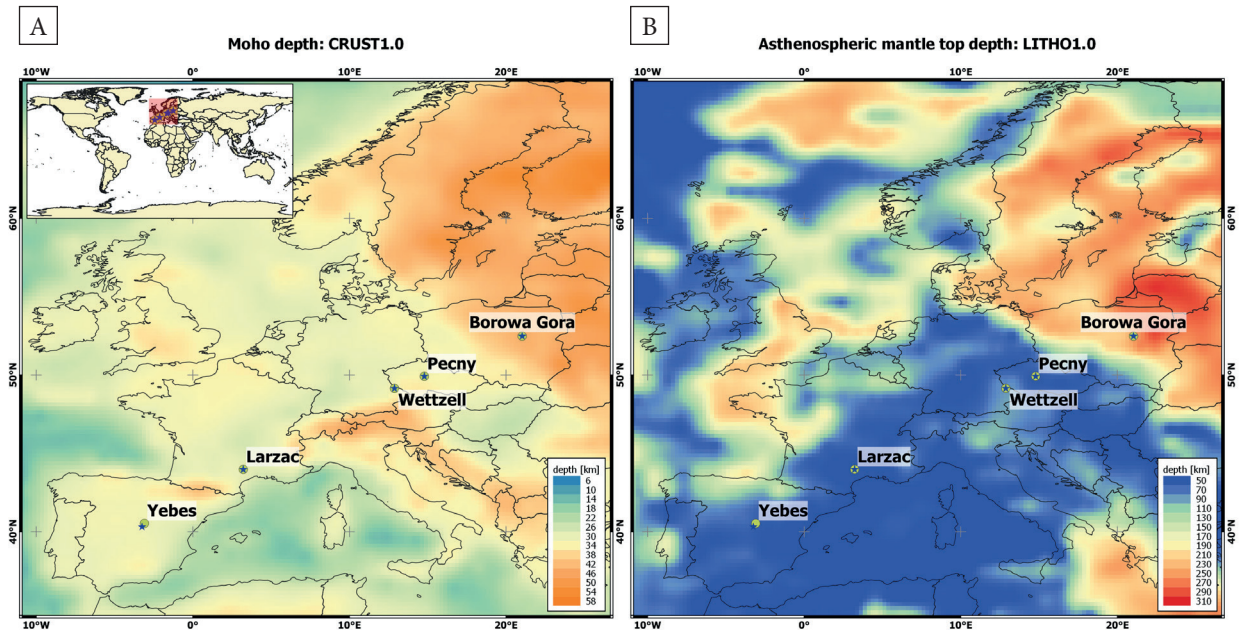
Fig. 2. *Moho depth after Laske et al. 2013 (A) and asthenosphere mantle top depth which corresponds to the lithosphere-asthenosphere boundary after Pasyanos et al. 2014 (B) of the analysed region and their surroundings; location of gravimetric stations are marked by stars and seismic ones by dots*

A slightly different image of V_s perturbation along the analysed profile with respect to the PREM model was obtained by Peter et al. (2008) based on a global phase-anomaly database of intermediate- to long-period Rayleigh waves. Their finite-frequency shear-velocity model of the European-Mediterranean region for depths between 100–400 km provides anomalies of higher magnitude (even up to −6%) located mainly in the Iberian Peninsula and Central Europe.

A global 3-D SV-wave tomographic model of the upper mantle down to the depth of 650 km based on the modelling of the fundamental and higher-mode Rayleigh waveforms was developed by Debayle & Ricard (2012). Along the profile of this study, they observed no velocity contrasts larger than ±0.5% below the depth of 250 km relative to the PREM model, except for a high positive velocity anomaly (+3%) at the depth of 450–550 km in southern France/northern Italy. What is more, their average 1-D velocity model was very close to the initial PREM model.

Continuous seismometric data have been downloaded through the European Integrated Data Archive (http://www.orfeus-eu.org/data/eida/; last access: April 2022) and gravimetric data from

the IGETS database (https://isdc.gfz-potsdam.de/igets-data-base; last access: August 2021). The typical sampling rate of SG data is 1 s but uploading 1-second data to the IGETS database is still not common. Routinely, 1-minute pre-processed gravimetric data are reported there. As earthquakes are seen as disturbances in gravimetric recordings, some operators use filters or other techniques to remove them. In such cases, retrieving an original signal to analyse earthquake waveforms is impossible. Fortunately, it is not the case for all IGETS's stations. For the selected stations, 1-second data are available. 1-minute data are in the end used only for SG from Wettzell and Pecny Observatory because 1-second data are available only for a short period, and simultaneously, 1-minute data are characterised by undistorted earthquake recordings.

The other limitation of using gravimetric data in studying earthquake waveforms is the unavailability of most gravimeters' transfer functions. The instrument response commonly used in seismology is rarely performed in gravimetric studies. There are only files with calibration factors and the time lags of gravimeters in the IGETS database. The assumption is made that those values

are constant for all recorded periods. In fact, it is only valid for periods above 100–200 s, depending on the type of gravimeter employed (see e.g., Karkowska et al. 2022a) while, especially for periods below 100 s, the coefficients can vary significantly. Therefore, a joint analysis of seismometric and gravimetric data is proposed in this paper, for short as well as long periods in order to resolve this problem.

A list of global earthquakes with a magnitude greater than 3.0 based on the bulletin of earthquakes downloaded from the EMSC service (https://www.emsc-csem.org/, last access: September 2021) was prepared, considering the location of the selected stations. The European bulletin was used to ensure the proper determination of parameters of earthquakes from Europe and its surroundings. Earthquakes that occurred from July 2013 until the end of 2020 were selected. Earthquakes whose records overlapped, as well as records for which the signal-to-noise ratio was below 1.6 and the amplitude ratio lower than 1.45, were removed from the list. The noise and signal were chosen to be a waveform before and after (including surface waves) the theoretical time of arrival of the longitudinal volumetric wave (P), respectively. The final number of analysed events for each station is presented in Table 1. An example of the distribution of earthquake epicentres for the Borowa Góra station is presented in Figure 3, together with the distribution of backward azimuth of the analysed events. Histograms of backward azimuth for other stations are presented in the "Supplementary material" section (Fig. S1).

The data processing procedure included the following:

1. Detrending, tapering, and filtering of analysed data. The BB data were filtered by the zero-phase Butterworth bandpass filter of 4th order and period corners of 2–1000 s. SG data were filtered in the same way, but with period corners of 10–1000 s for 1-second data and with period corners of 120–1000 s for 1-minute data. Additionally, the full instrument responses were removed from the BB data together with their differentiation and resampling to 1 s to create a consistent dataset of seismometric and gravimetric data. The 1-minute SG data were resampled to 1 s. Finally, SG recordings were corrected by a calibration factor and time lag. The BB data cut-off used for period corner of 1000 s was far away from the recording bandpass of instruments, but it was applied to maintain consistency in the proposed procedure. Possible effects of numerical amplifying of the noise resulting from such a wide filtering range were removed in the later steps of the proposed method, during the selection of the calculated group velocities. For a detailed analysis of the characteristics of gravimeters transfer functions and data processing see Karkowska et al. (2022a).

2. Determination of the group velocity dispersion curve for the fundamental mode of the Rayleigh wave was done using a frequency time analysis (FTAN) introduced by Dziewonski et al. (1969) and later perfected by Keilis-Borok (1989). One hundred Gaussian filters of central periods in the range of 2–1000 s, 10–1000 s, and 120–1000 s were applied for BB, SG 1-second and SG 1-minute data, respectively.

3. Estimation of mean surface dispersion curve (SWD) with standard deviation for each station for two cases: based on the BB data only (BB SWD) and also on the joint BB and SG data (BB+SG SWD) by applying two criteria proposed by Soomro et al. (2016). The first criterion is the background model criterion, allowing the maximum difference of 10% between the estimated mean group velocity of each period and the one calculated based on the ak135 model (Kennett et al. 1995). The second criterion is the smoothness criterion based on the normalised summed difference of the first derivative of the estimated and ak135 group velocities in the assumed period range. In the case of joint BB and SG data, one combined SWD and probability density distribution were calculated (using BB data up to 300 s, SG – from 100 s). As a reference, the probability density maps were also used to better assess the SWD reliability and to exclude potential numerical artefacts. The probability density distribution of group velocity at each period for each station was estimated based on all individual dispersion curves. All of the probability density maps are presented in the "Supplementary material" section (Fig. S2).
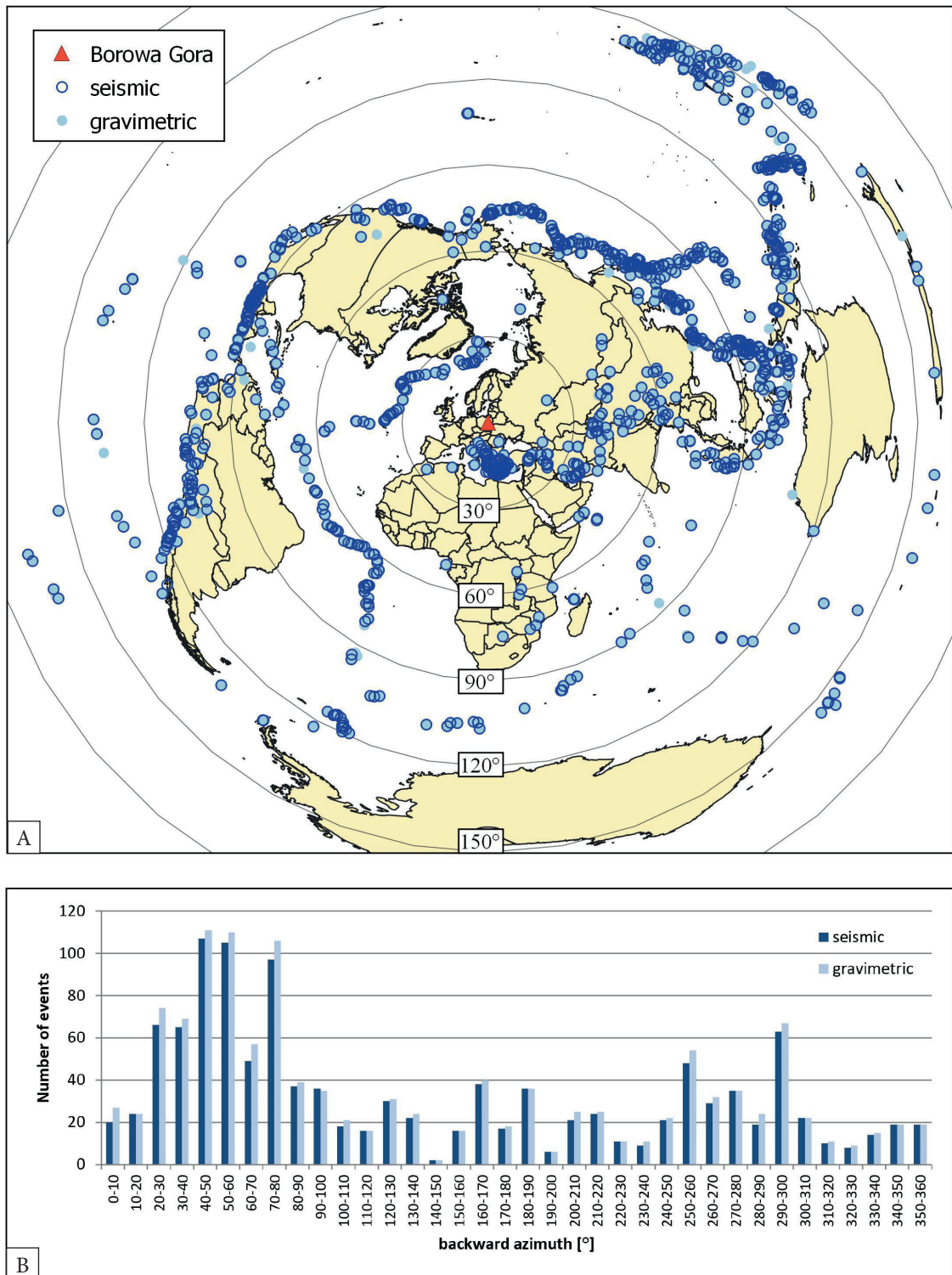
Fig. 3. *The distribution of earthquake's epicentres for the Borowa Góra station (A) together with the distribution of backward azimuth of analysed events (B)*

The Earth's seismic structure can be estimated by applying an inversion method to the calculated dispersion curve. Reliable values of group velocities must be selected to carry out the inversion procedure. Additionally, a dispersion curve must have no discontinuities.
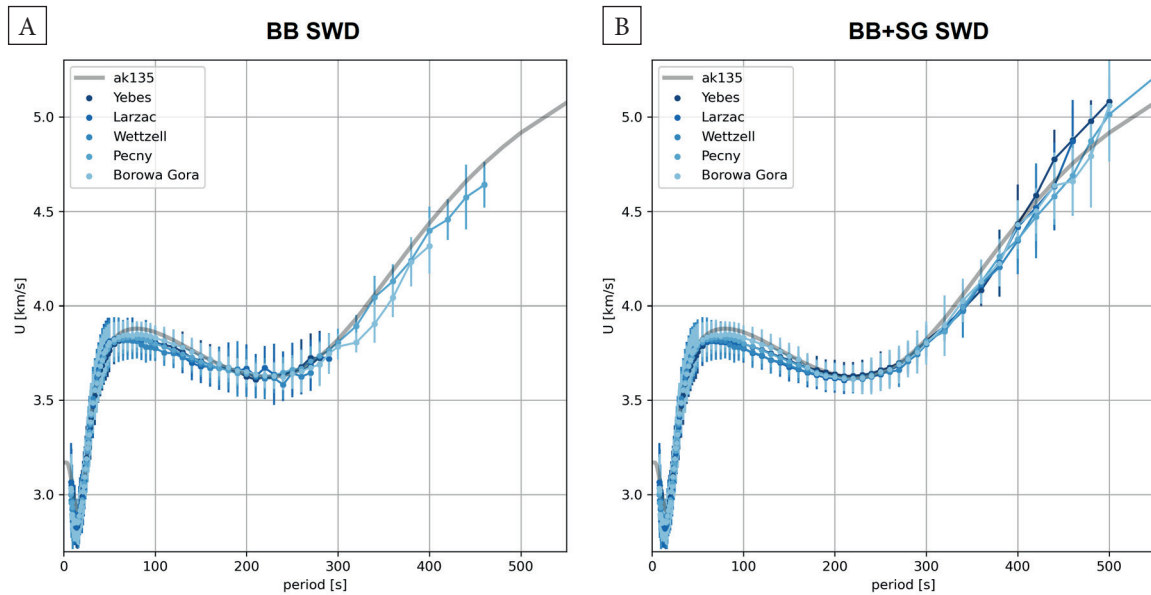
Fig. 4. *Final mean group-velocity dispersion curves of fundamental Rayleigh waves (solid lines in blue tones) with standard deviation (bars) calculated based on seismometric (BB SWD) (A) and joint seismometric and gravimetric (BB+SG SWD) (B) recordings for selected sites. The dispersion curve calculated for the ak135 model is shown by grey line*

The smallest value of the period used in the inversion procedures is determined as 8 s for all dispersion curves because non-smoothness and gaps in curves for shorter periods are often observed. The largest value of the period used in the inversion was determined based on the continuity criterion. Some values may have been rejected if the continuity criterion is not fulfilled. Additionally, the quality of dispersion curves was verified with the probability density map (see "Supplementary material" – Fig. S2). The final mean dispersion curves with standard deviations are shown in Figure 4.

In the case of the BB data, smooth and reliable dispersion curves are observed up to 200 s. The exceptions are curves estimated based on the BB data from the Pecny and Wettzell stations, which seem credible even up to 300 s. In the case of the joint BB and SG data, the dispersion curves are reliable up to 400 s. Generally, for longer periods, values of group velocities can only be determined for a small number of earthquakes. A few events with recordings of surface waves with good visible seismic energy in periods above 400 s can be identified. For example, in the case of BB+SG SWD for the Wettzell station, in a period range of 12–250 s, the number of samples used to calculate the mean

dispersion curves is above 500 with the maximum number of samples at the period of 50 s reaching 2613. Outside this range, the number of samples decreases rapidly until it reaches 0.

In the present paper, the recordings of regional-to-teleseismic global earthquakes are analysed and mean dispersion curves calculated for each station. Thus, the resulting curves can describe the average Earth's structure. However, the differences between them can be seen (up to a period of 170 s) arising from the location of the stations within a radius of 300–600 km. Generally, all dispersion curves are close to the dispersion curve calculated for the ak135 model (Kennett et al. 1995) with observed differences of −3% to 5%.

RESULTS OF WEIGHTED LINEAR INVERSION

A weighted linear inversion algorithm from the Computer Programs in the Seismology package (Herrmann 2013) was applied to estimate the Earth's seismic structure based on the calculated final mean dispersion curves (BB SWD and BB+SG SWD). The 1-D model of the subsurface is constituted of a stack of homogeneous linear elastic layers with a thickness of 20 km. A ratio of

Determination of the seismic structure of the Earth based on joint analysis of gravimetric and seismometric data – a case study

13

P-wave velocity to S-wave velocity (V_P/V_S) in each layer is assumed to be the same as in the ak135 initial model. The density of the medium in each layer was calculated according to the Nafe–Drake formula (Herrmann & Ammon 2004). The ak135 model was taken as a starting (initial) model with a maximum depth of 2800 km and then adjusted in 50 iterations to obtain the final model according to the best-fit criterion. In each iteration, the smoothing procedure was also applied by implementing a differential smoothing of velocities between the adjacent layers, which helped to stabilize an underdetermined problem (see details of LIN method in Herrmann & Ammon 2004). An example of dispersion curves with the standard deviation and results of inversion together with sensitivity kernels for the Borowa Góra station are shown in Figure 5. The sensitivity kernels, a partial derivative of group velocity dispersion (δU) with respect to S-wave velocity (δV_S) clearly show that surface waves of long periods are more sensitive to deeper structures of the Earth, e.g., surface waves of a period of 500 s can provide information about the Earth's seismic structure even up to the depth of 1000–1200 km. Results for other stations are shown in the "Supplementary material" section (Fig. S3).

Resolution matrices evaluate the results of weighted linear inversion. These matrices show the sensitivity of the dispersion curves to the model parameters and the inversion scheme. The resolution matrices are calculated for all inverted models for all stations. Figure 6 shows the resolution matrices with maximum and optimum resolution depths marked with black and red stars, respectively. The maximum resolution depth was estimated as the depth for which the value of the resolution matrix exceeds zero along diagonal, searching from the deepest layers. The optimum resolution depth is the depth on the vertical axis for which the maximum of deepest observed amplitude contour is reached. Table 2 summarizes the maximum period of each calculated mean dispersion curve together with resolution depths estimated based on resolution matrices (maximum and optimum values). Due to the asymmetry in the resolution matrix caused by the smoothing procedure, the optimum resolution depth is not linearly proportional to the maximum period of the mean dispersion curve. Nevertheless, the larger the maximum period, the deeper the structures which are retrieved in the inversion procedure.

Figure 7 shows all final models retrieved based on joint seismometric and gravimetric dispersion curves (BB+SG SWD). As a reference, the initial ak135 model is also presented. The differences between resulting models and the ak135 model are small, generally ranging from −3% to 6%. The obtained velocities in the crust and upper mantle are smaller than in the ak135 model, with a maximum absolute difference of 3% and 2%, respectively. In the lower mantle, the residuals vary from −2% to 6%.
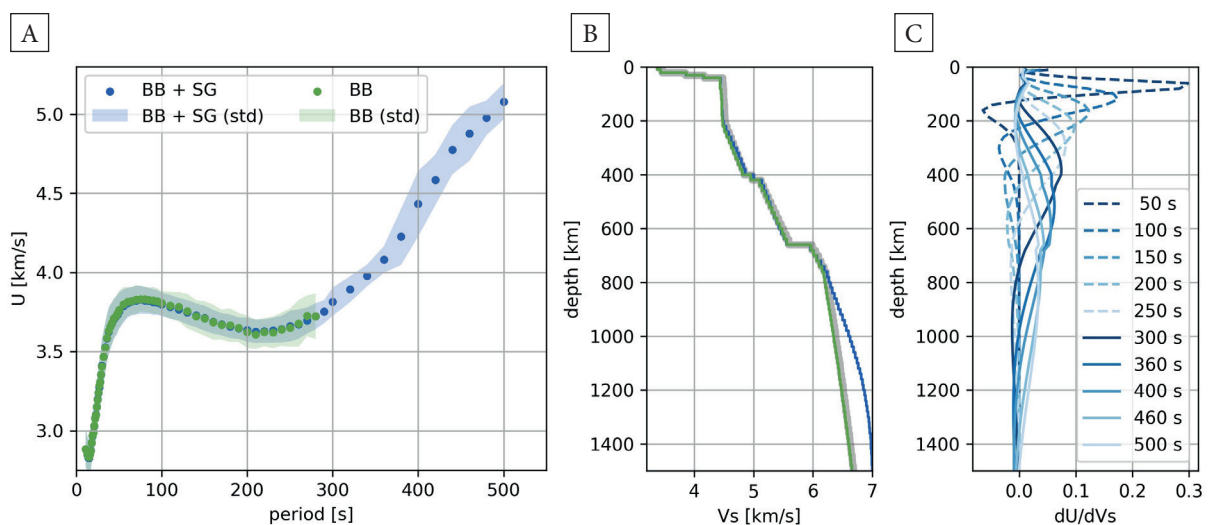

Fig. 5. *Final mean group-velocity dispersion curves of fundamental-mode Rayleigh waves with the standard deviation (A), results of inversion together with the initial ak135 (B) and sensitivity kernels (C) for the Borowa Góra station*
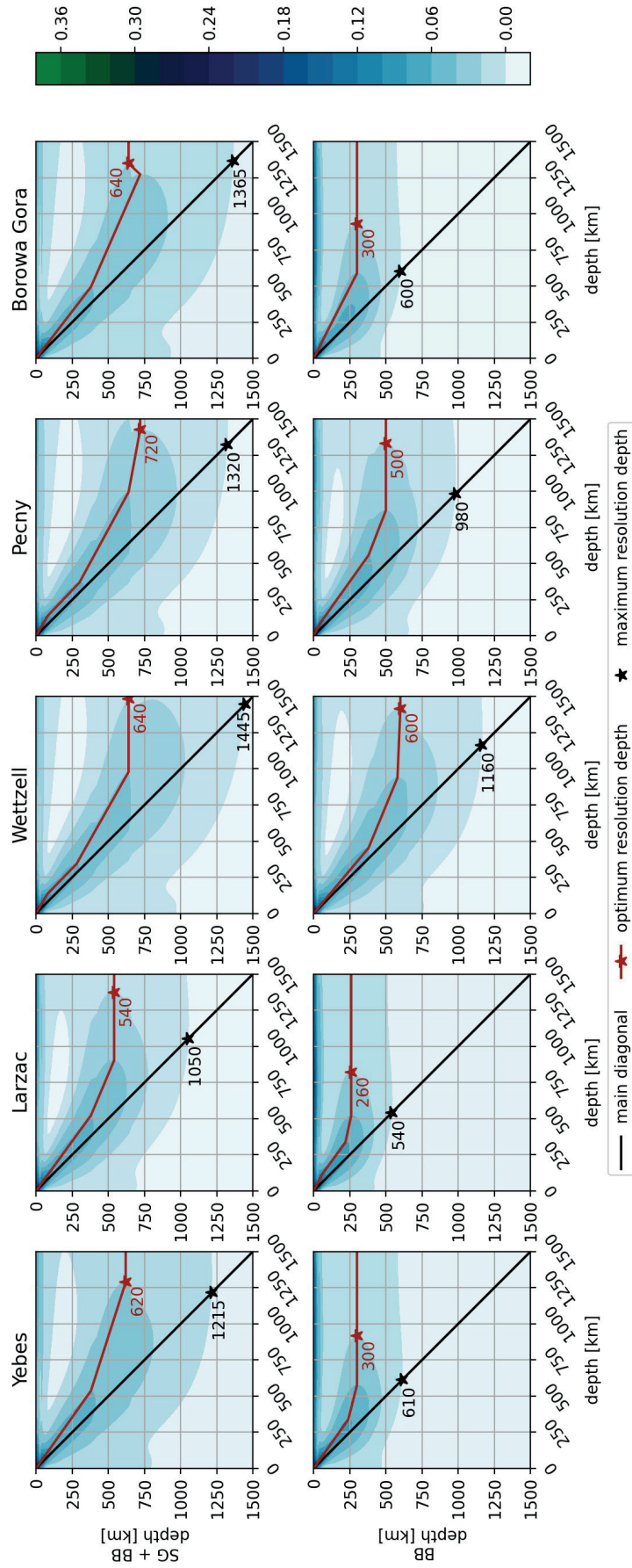
Fig. 6. *Resolution matrices of the inversion scheme for the BB and the joint (BB+SG) dispersion curves for all selected stations: Yebes, Larzac, Wettzell, Pecny and Borowa Góra (from left to the right panel); a maximum resolution depth is marked with a black star and an optimum resolution depth with a red star*

List of selected stations with the maximum period of their dispersion curves and optimum and maximum resolution depths of the weighted linear inversion method

Parameter	Yebes		Larzac		Wettzell		Pecny		Borowa Góra	
	BB	BB+SG	BB	BB+SS	BB	BB+SG	BB	BB+SG	BB	BB+SG
Maximum period [s]	290	460	270	420	460	550	400	480	280	500
Optimum depth [km]	300	620	260	540	600	640	500	720	300	640
Maximum depth [km]	610	1215	540	1050	1160	1445	980	1320	600	1365
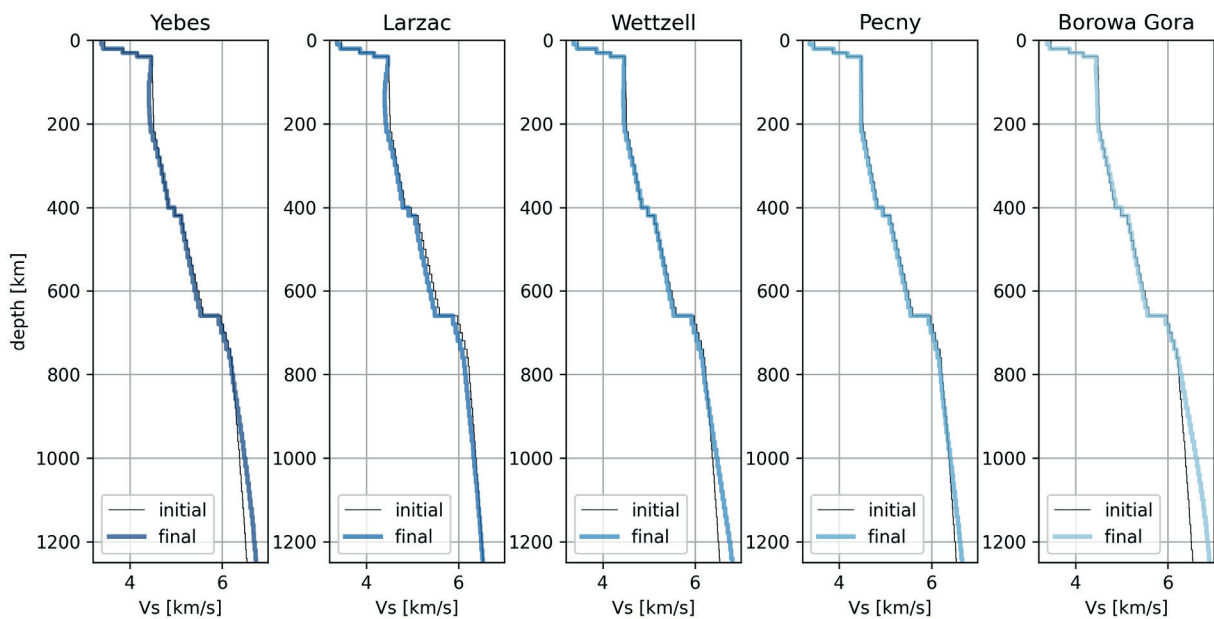
Fig. 7. *Results of linear inversion method (final model) of joint dispersion curves of a fundamental-mode Rayleigh wave for all selected stations together with the initial ak135 model*

RESULTS OF MONTE CARLO INVERSION

Additionally, the transdimensional reversible-jump Markov chain Monte Carlo (rj-McMC) method of Bodin et al. (2012) was used to estimate the Earth structure based on the joint dispersion curves of Rayleigh waves (BB+SG SWD). The main advantage of the rj-McMC method is its ability to not only determine seismic velocities but also a model dimension (number of parameters) and data noise level during the inversion procedure. Samples are generated from an a priori uniform distribution within a V_S range of 2.75–8.25 km/s. The inversion procedure is performed down to

a depth of 1250 km, the average value of maximum resolution depth of weighted linear inversion for joint (BB+SG) dispersion curves (see Table 2). The initial thickness of the layers is 12.5 km. The V_P/V_S ratio of the medium is assumed as a constant in each layer and set to 1.73, while the density is calculated based on the Nafe–Drake formula (Ludwig et al. 1970). The total number of iterations of the reversible jump algorithm is $2 \cdot 10^6$, and the first half is discarded as burn-in steps.

Figure 8 shows the posterior approximation of true models – the posterior probability distribution of V_S at each depth, where the white colour indicates the high probability of a particular value of V_S.
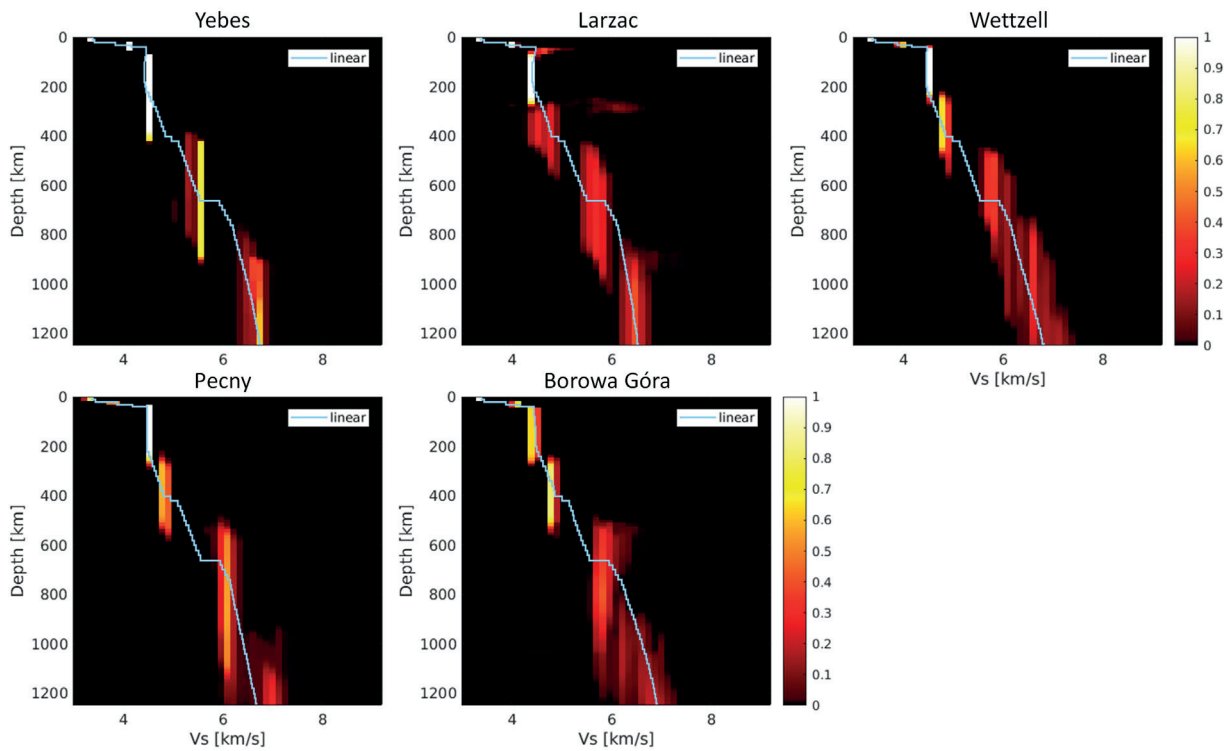
Fig. 8. *Results of the Monte Carlo inversion of joint dispersion curves of a fundamental-mode Rayleigh wave for all selected stations together with the final linear inversion model (marked as light blue line). The plots represent the posterior probability distribution of S-wave velocity (V_S) at each depth. The white colour shows high probabilities and the red indicates low probabilities*

The Monte Carlo inversion results show that only up to 6–7 almost homogeneous layers of the crust and the mantle down to the depth of 1250 km can be distinguished based on the dispersion curves of the fundamental mode of Rayleigh waves. Generally, the most probable values of V_S at each depth follow the values obtained from the weighted linear inversion (marked using a light blue line in Figure 8). However, the probability of the most probable values of V_S is only higher than 0.5 over the entire range of depths for the Yebes and Pecny stations. In the case of the Larzac station, the most probable V_S are only reliable down to a depth of 300 km – below that depth, the probability of V_S is smaller than 0.3.

DISCUSSION

The joint seismometric and gravimetric dispersion curves can be used to retrieve a reliable model of the crust and upper mantle thanks to seismometric data as well as the lower mantle thanks to gravimetric data. Using both seismometric and gravimetric data allows the calculation of dispersion curves even up to 550 s. While, for the same area, the maximum analysed period from seismometric data by Peter et al. (2008), Schivardi & Morelli (2011), Debayle & Richard (2012) was 300 s, 170 s and 200 s, respectively.

Generally, the weighted linear inversion models presented in this study are consistent with the global ak135 model. That should be an expected result, given that the inverted dispersion curves for each site were calculated for the global distribution of earthquakes and that the ak135 model describes the continental structure well. Furthermore, the data used for all stations are characterized by a good uniform back azimuthal distribution of events (see the "Supplementary material" section – Fig. S1). However, some differences in the weighted linear inversion models can be seen which can be explained by the regional models

developed by Peter et al. (2008), Schivardi & Morelli (2011), and Debayle & Richard (2012). In the presented study, the weighted linear inversion models show velocities lower by 2% relative to the ak135 model at a depth range of 110–230 km below the Yebes and Larzac stations and lower by 2% at a depth range of 490–740 km below the Larzac station. These features are also visible in the regional models, but they are more emphasized here. It should be remembered that models below the optimum resolution depth (500–720 km) might be less reliable because of the decreasing value of the sensitivity kernels ($\delta U/\delta V_S$) with the depth. The increase of S-wave velocity with respect to the ak135 model for the Yebes and the Larzac stations below the depth of 1000 km and for the Borowa Góra station below the depth of 800 km, may also show that the estimated averaged dispersion curves for longer periods in those cases need to be verified.

The resolution abilities of surface waves are well demonstrated by the Monte Carlo inversion results, where only 6–7 almost homogenous layers can be detected down to the depth of 1250 km. The obtained models are quite similar to one another, apart from two cases: (1) for the Yebes station, an increase of seismic velocities is not observed at the depth of 270–310 km as for other stations, but at the depth of 450 km and (2) for the Pecny station, velocities below the depth of 490 km are much larger than observed for other stations. Schivardi & Morelli (2011) have reported negative velocity anomalies down to the depth of 250 km in the area of the Yebes and Larzac stations. Also, Peter et al. (2008) have presented distinctive V_S perturbations of –2% and –4% in the Iberian Peninsula with respect to the PREM model at the depths of 220–310 km, and 310–400 km, respectively. The estimated high velocities below the depth of 490 km for the Pecny station are not reported in previous studies and might be the result of overestimated velocity values for periods longer than 400 s (see the "Supplementary material" section). Generally, the resulting seismic velocities below the depth of 800 km may be less reliable due to a small number of group-velocity measurements for periods longer than 400 s.

CONCLUSIONS

This study presents a new concept for the joint analysis of the gravimetric and seismometric recordings of earthquakes to determine dispersion curves of the fundamental mode of Rayleigh surface waves up to a period of 550 s. The proposed method allows using gravimetric data without the known full transfer function of the instrument. Calculated dispersion curves can be inverted by the weighted linear inversion and Monte Carlo methods to estimate a distribution of shear-wave seismic velocity in the Earth even down to the depth of 1000–1200 km. In the case of linear inversion, the final model below the optimum resolution depth might follow the starting model while, in the case of Monte Carlo inversion, the velocities of the last layers for which the sensitivity of determined dispersion curves is non-negligible are prolonged to greater depths.

Generally, observed details in linear inversion models are unreliable due to the sensitivity of long-period surface waves. In fact, based on the presented analysis of the dispersion curve of the fundamental mode of Rayleigh waves, the seismic structure of the upper mantle can be modelled by 2–3 almost homogenous layers. Additionally, the models inverted based on averaged dispersion curves may largely estimate an averaged 1-D seismic model of the Earth better than the local structures around the stations. The local structure determination will be the subject of further studies, in which two-station method will be applied.

Tidal gravimeters also provide a unique opportunity to verify the seismometric recordings of earthquakes at long periods (above 120 s). Consequently, gravimetric data can complement seismometric recordings for longer periods, depending on the seismometer type and its cut-off period. A superconducting gravimeter can act as a single (vertical) component of a very broad-band seismometer.

REFERENCES

Bodin T., Sambridge M., Tkalčić H., Arroucau P., Gallagher K. & Rawlinson N., 2012. Transdimensional inversion of receiver functions and surface wave dispersion. *Journal of Geophysical Research*, 117(B2), B02301. https://doi.org/10.1029/2011JB008560.

Bormann P., Engdahl E. & Kind R., 2012. Seismic Wave Propagation and Earth Models. [in:] Bormann P. (ed.), *New Manual of Seismological Observatory Practice 2 (NMSOP-2)*, Deutsches GeoForschungsZentrum GFZ, Potsdam, 15–27. https://doi.org/10.2312/GFZ.NMSOP-2_ch2.

Charles University in Prague (Czech), Institute of Geonics, Institute of Geophysics, Academy of Sciences of the Czech Republic, Institute of Physics of the Earth Masaryk University (Czech) & Institute of Rock Structure and Mechanics, 1973. *Czech Regional Seismic Network* [Data set]. International Federation of Digital Seismograph Networks. https://doi.org/10.7914/SN/CZ.

Debayle E. & Ricard Y., 2012. A global shear velocity model of the upper mantle from fundamental and higher Rayleigh mode measurements. *Journal of Geophysical Research*, 117, B10308. https://doi.org/10.1029/2012JB009288.

Dercourt J., Zonenshain L.P., Ricou L.-E., Kazmin V.G., Le Pichon X., Knipper A.L., Grandjacquet C., Sbortshikov I.M., Geyssant J., Lepvrier C., Pechersky D.H., Boulin J., Sibuet J.-C., Savostin L.A., Sorokhtin O., Westphal M., Bazhenov M.L., Lauer J.P. & Biju-Duval B., 1986. Geological evolution of the Tethys belt from the Atlantic to the Pamirs since the LIAS. *Tectonophysics*, 123(1–4), 241–315. https://doi.org/10.1016/0040-1951(86)90199-X.

Dykowski P., Sekowski M. & Krynski J., 2018. *Superconducting gravimeter data from Borowa Gora – Level 1*. GFZ Data Services. https://doi.org/10.5880/igets.bg.l1.001.

Dziewonski A. & Anderson D., 1981. Preliminary reference Earth model. *Physics of the Earth and Planetary Interiors*, 25, 297–356. https://doi.org/10.1016/0031-9201(81)90046-7.

Dziewonski A., Bloch S. & Landisman M., 1969. A technique for the analysis of transient seismic signals. *Bulletin of the Seismological Society of America*, 59(1), 427–444. https://doi.org/10.1785/BSSA0590010427.

Federal Institute for Geosciences and Natural Resources (BGR), 1976. *German Regional Seismic Network (GRSN)*. Bundesanstalt für Geowissenschaften und Rohstoffe. https://doi.org/10.25928/mbx6-hr74.

Gaudot I., Beucler É., Mocquet A., Drilleau M., Haugmard M., Bonnin M., Aertgeerts G. & Leparoux D., 2021. 3-D crustal V_S model of western France and the surrounding regions using Monte-Carlo inversion of seismic noise cross-correlation dispersion diagrams. *Geophysical Journal International*, 224(3), 2173–2188. https://doi.org/10.1093/gji/ggaa552.

Herrmann R.B., 2013. Computer programs in seismology: An evolving tool for instruction and research. *Seismological Research Letters*, 84(6), 1081–1088. https://doi.org/10.1785/0220110096.

Herrmann R.B. & Ammon C.J., 2004. *Surface waves, receiver functions and crustal structure, Computer Programs in seismology: version 3.30*. Saint Louis University.

Hunter J., 2007. Matplotlib: A 2D graphics environment. *Computing in Science & Engineering*, 9(3), 90–95. https://doi.org/10.1109/MCSE.2007.55.

Karkowska K. & Wilde-Piórko M., 2022. Determination of the Earth's structure based on intermediate-period surface wave recordings of tidal gravimeters: A case study. *Earth, Planets and Space*, 74, 150. https://doi.org/10.1186/s40623-022-01712-4.

Karkowska K., Wilde-Piórko M. & Dykowski P., 2022. Analysis of earthquakes recordings of tidal gravimeters in the period range of 10–1000 s. *Acta Geodynamica et Geomaterialia*, 19(1), 79–92. https://doi.org/10.13168/AGG.2021.0043.

Keilis-Borok V.I., 1989. Recording, identification, and measurement of surface wave parameters. [in:] Keilis-Borok V.I. (ed.), *Seismic Surface Waves in a Laterally Inhomogeneous Earth*, Modern Approaches in Geophysics, 9, Kluwer Academic Publishers, Dordrecht, 131–182. https://doi.org/10.1007/978-94-009-0883-3_5.

Kennett B.L.N., Engdahl E.R. & Buland R., 1995. Constraints on seismic velocities in the Earth from travel times.

Geophysical Journal International, 122(1), 108–124. https://doi.org/10.1111/j.1365-246X.1995.tb03540.x.

Kolínský P., Valenta J. & Málek J., 2014. Velocity model of the Hronov-Poříčí Fault Zone from Rayleigh wave dispersion. *Journal of Seismology*, 18(3), 617–635. https://doi.org/10.1007/s10950-014-9433-4.

Köhler A., Maupin V. & Balling N., 2015. Surface wave tomography across the Sorgenfrei–Tornquist Zone, SW Scandinavia, using ambient noise and earthquake data. *Geophysical Journal International*, 203(1), 284–311. https://doi.org/10.1093/gji/ggv297.

Krischer L., Megies T., Barsch R., Beyreuther M., Lecocq T., Caudron C. & Wassermann J., 2015. ObsPy: a bridge for seismology into the scientific Python ecosystem. *Computational Science & Discovery*, 8(1), 014003. https://doi.org/10.1088/1749-4699/8/1/014003.

Laske G., Masters G., Ma Z. & Pasyanos M., 2013. Update on CRUST1.0 – A 1-degree Global Model of Earth's Crust. [in:] *Geophysical Research Abstracts. Vol. 15: EGU General Assembly 2013, 7–12 April, 2013, Vienna, Austria*, EGU2013-2658.

Ludwig W.J., Nafe J.E. & Drake C.L., 1970. Seismic refraction. [in:] Maxwell A.E. (ed.), *The Sea: Ideas and Observations on Progress in the Study of the Seas. Volume 4: New Concepts of Sea Floor Evolution. Part One*, Wiley-Interscience, New York, 53–84.

Lyu Ch., Pedersen H.A., Paul A., Zhao L., Solarino S. & CIFALPS Working Group, 2017. Shear wave velocities in the upper mantle of the Western Alps: New constraints using array analysis of seismic surface waves. *Geophysical Journal International*, 210(1), 321–331. https://doi.org/10.1093/gji/ggx166.

Martínez M.D., Lana X., Caselles O., Canas J.A. & Pujades L., 2005. Elastic-anelastic regional structures for the Iberian Peninsula obtained from a Rayleigh wave tomography and a causal uncoupled inversion. *Pure and Applied Geophysics*, 162(12), 2321–2353. https://doi.org/10.1007/s00024-005-2778-4.

Pálinkáš V., Kostelecký J. & Vaľko M., 2020. *Superconducting gravimeter data from Pecný – Level 1*. GFZ Data Services. https://doi.org/10.5880/igets.pe.l1.001.

Pasyanos M.E., Masters T.G., Laske G. & Ma Z., 2014. LITHO1.0: An updated crust and lithospheric model of the Earth. *Journal of Geophysical Research*, 119(3), 2153–2173. https://doi.org/10.1002/2013JB010626.

Pawlewicz M.J., Williams A.J., Walden S.M. & Steinshouer D.W., 2003. *Generalized Geology of Europe including Turkey (geo4_2l)*. U.S. Geological Survey data release, https://doi.org/10.5066/P9C8ZY5Q.

Peter D., Boschi L., Deschamps F., Fry B., Ekström G. & Giardini D., 2008. A new finite-frequency shear-velocity model of the European-Mediterranean region. *Geophysical Research Letters*, 35(16), L16315. https://doi.org/10.1029/2008GL034769.

Pharaoh T.C., 1999. Palaeozoic terranes and their lithospheric boundaries within the Trans-European Suture Zone (TESZ): A review. *Tectonophysics*, 314(1–3), 17–41. https://doi.org/10.1016/S0040-1951(99)00235-8.

QGIS.org, 2020. *QGIS Geographic Information System*. QGIS Association. http://www.qgis.org.

RESIF, 1995. *RESIF-RLBP French Broad-band network, RESIF-RAP strong motion network and other seismic stations in metropolitan France* [Data set]. RESIF – Réseau Sismologique et géodésique Français. https://doi.org/10.15778/RESIF.FR.

Romanowicz B., 2002. Inversion of surface waves: a review. [in:] Lee W.H.K., Jennings P., Kisslinger C., Kanamori H. (eds.), *International Handbook of Earthquake & Engineering Seismology, Part A*, Academic Press, Cambridge, 149–173. https://doi.org/10.1016/S0074-6142(02)80214-5.

San Fernando Royal Naval Observatory (ROA), Universidad Complutense De Madrid (UCM), Helmholtz-Zentrum Potsdam Deutsches GeoForschungsZentrum (GFZ), Universidade De Évora (UEVORA, Portugal), & Institute Scientifique of Rabat (ISRABAT, Morocco), 1996. *The Western Mediterranean BB seismic Network* [Data set]. Deutsches GeoForschungsZentrum GFZ. https://doi.org/10.14470/JZ581150.

Schivardi R. & Morelli A., 2011. EPmantle: A 3-D transversely isotropic model of the upper mantle under the European Plate. *Geophysical Journal International*, 185(1), 469–484. https://doi.org/10.1111/j.1365-246X.2011.04953.x.

Shapiro N.M., Gorbatov A.V., Gordeev E. & Dominguez J., 2000. Average shear-wave velocity structure of the Kamchatka peninsula from the dispersion of surface waves. *Earth, Planets and Space*, 52(9), 573–577. https://doi.org/10.1186/BF03351665.

Soomro R.A., Weidle C., Cristiano L., Lebedev S., Meier T. & PASSEQ Working Group, 2016. Phase velocities of Rayleigh and Love waves in central and northern Europe from automated, broad-band, interstation measurements. *Geophysical Journal International*, 204(1), 517–534. https://doi.org/10.1093/gji/ggv462.

Wziontek H., Wolf P., Nowak I., Richter B., Rülke A. & Wilmes H., 2017. *Superconducting gravimeter data from Wettzell – Level 1*. GFZ Data Services. https://doi.org/10.5880/igets.we.l1.001.

SUPPLEMENTARY MATERIAL

Distributions of backward azimuth of all analysed events are presented in Figure S1. All histograms shows that the most frequent are events from north-east and south-west directions.

All estimated individual dispersion curves were used to create probability density distribution maps. Distribution maps for all stations are shown in Figure S2. On the left are maps based on broad-band seismic data (BB), while on the right side are based on both broad-band seismic and gravimetric data (BB+SG). The yellow indicates the high probability (above 0.9) of group-velocity values at a given period. The dispersion curves with the standard deviation and results of linear inversion together with sensitivity kernels for all stations are shown in Figure S3.
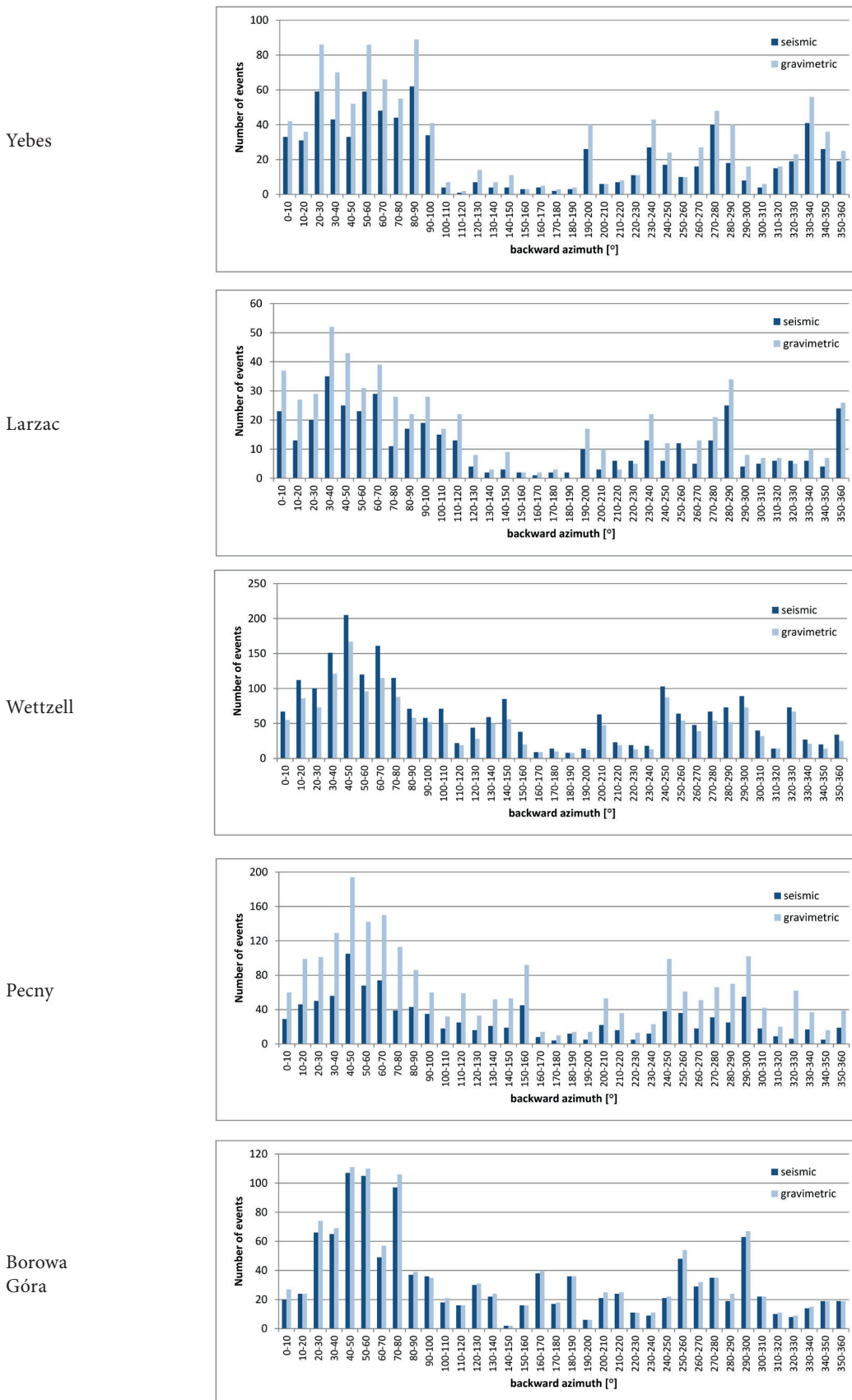
Yebes

Larzac

Wettzell

Pecny

Borowa
Góra

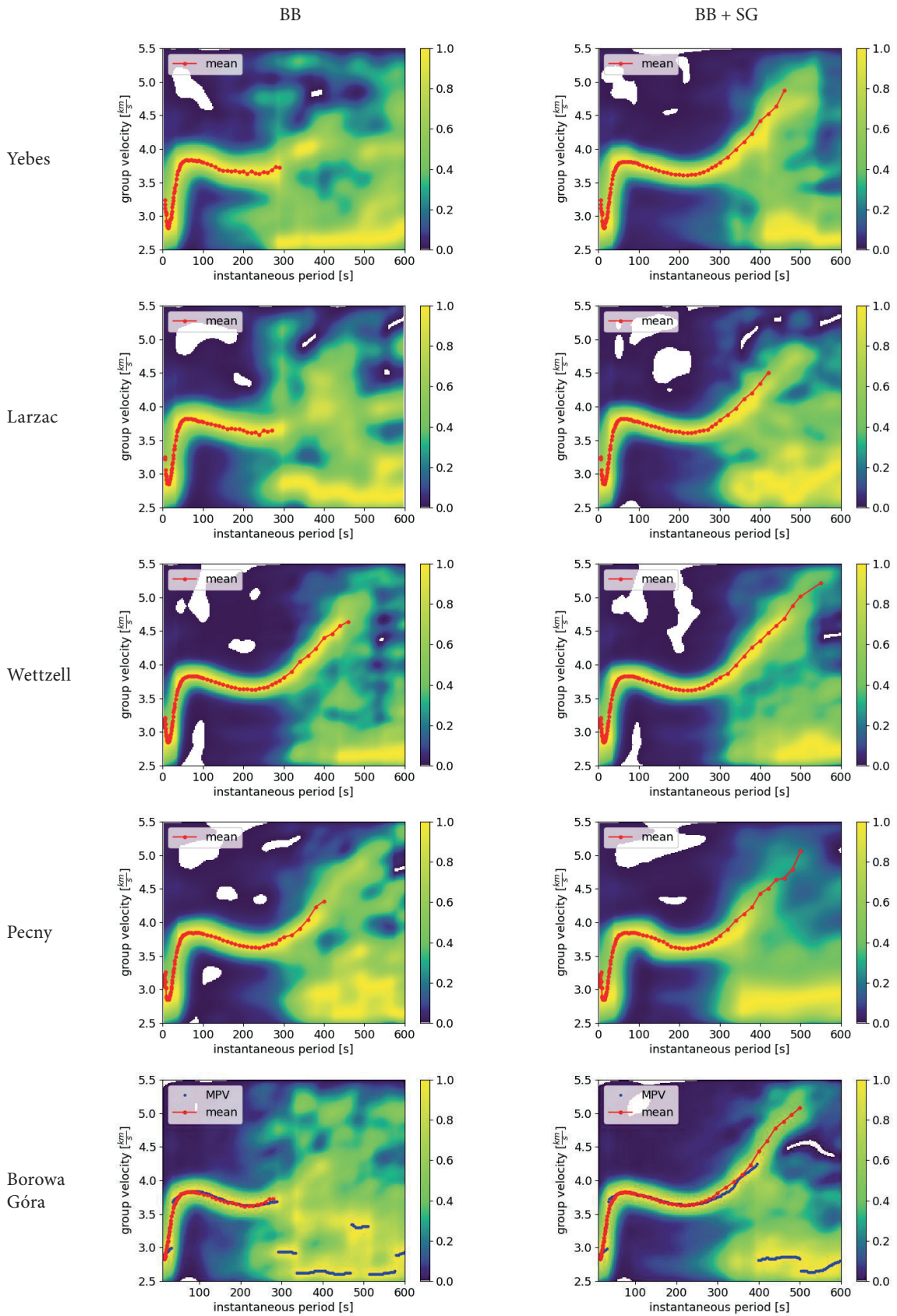**Fig. S1.** *Histograms of backward azimuth of all analysed events for all stations*

Fig. S2. *Distribution maps of group-velocity of fundamental-mode Rayleigh waves for broadband seismometer (BB) and joint curves, namely broad-band seismometer + superconducting gravimeters (BB+SG)*
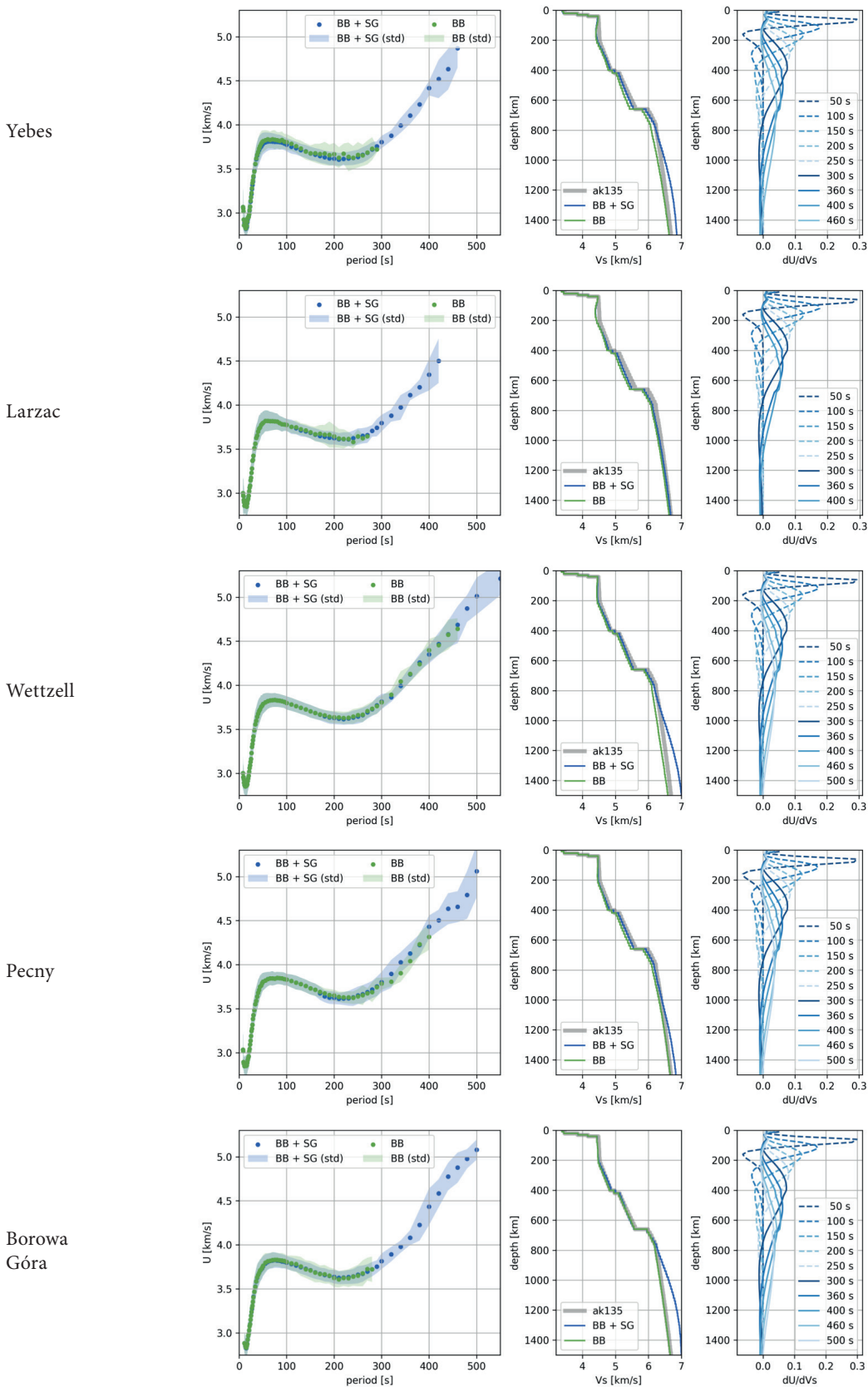
Fig. S3. *Final mean dispersion curves of a fundamental-mode Rayleigh waves with standard deviation (left panel), results of inversion together with the initial ak135 (middle panel) and sensitivity kernels for BB+SG (right panel) for all stations*